Aalborg Universitet

A Junction Temperature Monitoring Method for IGBT Modules Based on Turn-Off Voltage With Convolutional Neural Networks

Wang, Huimin; Xu, Zhiliang; Ge, Xinglai; Liao, Yongkang; Yang, Yongheng; Zhang, Yi; Yao, Bo; Chai, Yuheng

A Junction Temperature Monitoring Method for IGBT Modules Based on Turn-off Voltage with Convolutional Neural Networks

Huimin Wang, *Member, IEEE*, Zhiliang Xu, *Student Member*, *IEEE*, Xinglai Ge, *Member, IEEE*,
Yongkang Liao, Yongheng Yang, *Senior Member*, *IEEE*, Yi Zhang, *Member, IEEE*,
Bo Yao, *Student Member*, *IEEE*, and Yuheng Chai

Abstract-**Junction temperature monitoring (JTM) methods promise to perform reliability evaluation and health management for insulated-gate bipolar transistor (IGBT) modules, and thus are extensively focused on in power electronics converters. However, many JTM methods for IGBT modules are criticized for providing inaccurate junction temperature information with the problem of load current dependence. To address this, a JTM method based on the turn-off voltage (TOV) and convolutional neural networks (CNN) is proposed in this paper. In this method, the TOV is used as the junction temperature indicator, and the characterization behavior of the TOV during turn-off transient process is thoroughly analyzed. Then, the parameter dependence of the TOV is investigated. Considering the proposed JTM method may be subject to the issue of load current dependence and show an undesirable performance, the CNN is adopted to maintain the accuracy of junction temperature prediction due to its excellent global and local feature recognition capability. With this regards, the proposed JTM method enables accurate junction temperature information under different conditions. Finally, the double-pulse tests and experimental tests based on the test bench of a single-phase pulse-width modulation (PWM) rectifier are carried out to validate the effectiveness of the proposed JTM method.**

Index Terms-**Junction temperature monitoring (JTM), turn-off voltage, convolutional neural networks, load current dependence, insulated-gate bipolar transistor (IGBT)**

I. INTRODUCTION

Insulated-gate bipolar transistor (IGBT) modules are widely used in power electronics converters thanks to their features including high efficiency, high withstanding voltage, low turn-on voltage, and fast switching speed [1], [2]. Despite these attractive advantages, IGBT modules are identified as one of the most vulnerable components in power electronics converters due to harsh environment and complex conditions [3], [4]. One key issue degrading the reliability of the IGBT modules is the junction temperature swings. It has been investigated that the lifetime of the IGBT modules will be obviously affected by the junction temperature swings [5]-[7]. As such, accurate junction temperature monitoring (JTM) is strongly desirable for reliability evaluation and health management of IGBT modules. Considerable JTM methods are thus investigated in the literature and in industry as well.

The prior-art JTM methods typically can be divided into direct measurement methods [8], [9] and indirect estimation methods [10]-[30]. Though being effective in obtaining the junction temperature, the direct measurement methods are inapplicable in practice. This is because these methods require opening the shells of IGBT modules, and thus, may interrupt the proper operations of IGBT modules. Moreover, in the direct measurement methods, costly sensors are necessary to serve as junction temperature extractor. With this, concerns of reduced reliability and increased complexity should be carefully considered.

The indirect estimation methods enjoy the benefits of low invasiveness and high flexibility, and are of huge interest. Typically, the indirect estimation methods are implemented by the thermal network model-based methods [10]-[12] and the thermo-sensitive electrical parameter (TSEP)-based methods [13]-[30]. As for the thermal network model-based methods, their performance is dependent on the accuracy of the power loss calculation and the thermal network model. Moreover, a key challenge to these methods should be considered. That is, the heat dissipation and the aging of IGBT modules will cause an apparent performance deterioration, and this problem becomes more serious for long-term JTM. Though a few adaptive thermal models that take care of the aging effects have been reported in the literature, the issue of aging effect needs to be resolved well. Alternatively, the TSEP-based methods stand out among various JTM methods with relatively high accuracy and fast response. These methods exploit the electrical parameters of IGBT modules as the junction temperature indicator. Then, the task of JTM is accomplished by monitoring the electrical parameters.

As for the TSEP methods, the selection of electrical parameters is essential. Most popular JTM methods using the static TSEPs of IGBT modules have been proven to be available in the literature [13]-[20]. As detailed in [13], the collector-emitter voltage at low current levels was used to achieve the target of JTM. This method has a high linearity and avoids the effects of bond wire aging. However, due to low current levels, the availability of this method is questionable in practical applications. Following that, another attempt of the collector-emitter voltage at high current levels was further made to implement the task of JTM in [15]. Whereas, this method is susceptible to load current dependence and bond wire aging. Additionally, in [17], a JTM method based on the short-circuit current was presented, which allows an adequate sensitivity and linearity. Unfortunately, in this JTM method, a deliberately-designed

test circuit is required, which may cause additional complexity and cost. One interesting method monitoring the junction temperature of IGBT modules via the bus voltage ringing was reported in [18]. However, the JTM indicator is dependent on the load currents, which makes the performance of this JTM method afflicted with different load currents.

Research on the JTM methods has recently progressed with the introduction of the dynamic TSEP-based JTM methods [21]-[30]. Typical dynamic TSEPs include the maximum collector current falling rate [21], the turn-off delay time [22], the peak gate current [23], the dynamic threshold voltage [24], the flatband voltage [25], the pre-threshold voltage [26], the gate voltage plateau [27], and the voltage integral over voltage rise period [29]. Among them, [21] implemented a maximum collector current falling rate-based JTM method for IGBT modules. The junction temperature indictor is easy to measure from the intrinsic parasitic inductance of IGBT modules. Similarly, in [22], a JTM method using the turn-off delay time was proposed, in which this TSEP is also obtained from the intrinsic parasitic inductance. While, both JTM methods in [21] and [22] are burdened by the issue of load current dependence. Additionally, a JTM method based on the gate voltage plateau was investigated in [27]. Though feasible, the challenge in this JTM method is to show a high dependence of load currents. Moreover, in [29], the voltage integral over-voltage rise period that is obtained by a low frequency detection circuit, was assigned to extract the junction temperature, which benefits from a high accuracy and a low cost. A high-sensitivity JTM method by using the turn-on drain-source current overshoots was presented in [30], in which the performance of this method is insensitive to the changes of boundary conditions. Although the dynamic TSEP-based JTM methods remain attractive for IGBT modules, they can barely address the problem of load current dependence. Hence, innovative solutions are eagerly sought.

In light of the above, in this paper, a JTM method based on the turn-off voltage (TOV) and convolutional neural networks (CNN) is proposed for the IGBT modules, in which an achievement of load current independence is made and the information of the load current is not required. The rest of this paper is organized as follows. In Section II, the characterization behavior of the TOV during turn-off transient process is analyzed. Following that, an elaborated parameter dependence investigation of the TOV is developed, which is shown in Section III. It is revealed from the analysis that the TOV is possibly affected by load current dependence. Accordingly, in Section IV, the CNN is introduced in the proposed JTM method to address the problem of load current dependence. Then, the double-pulse tests and experimental tests based on the test bench of a single-phase pulse-width modulation (PWM) rectifier are carried out to extensively investigate the performance of the proposed JTM method under different operating conditions, and the results are presented in Section V and Section VI, respectively. Finally, Section VII concludes this paper.
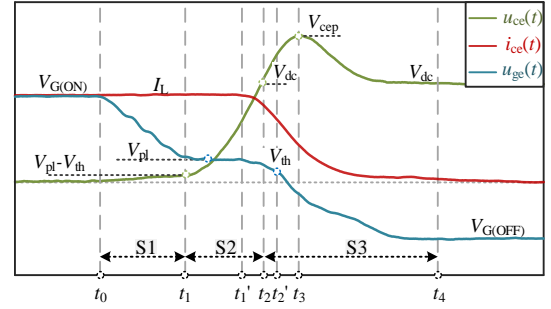

Fig. 1. Typical turn-off curves of the IGBT module (Infineon FF50R12RT4).

TABLE I
PARAMETERS OF THE IGBT MOUDLE (INFINEON FF50R12RT4)

Parameter	Value	Parameter	Value
$V_{G(ON)}$ (V)	15	V_{th} (V)	5.36
$V_{G(OFF)}$ (V)	-7.5	C_{ge} (nF)	2.7
R_{gi} (Ω)	4	C_{cg} (nF)	0.1
R_{ge} (Ω)	10	I_L (A)	50

II. CHARACTERIZATION BEHAVIOR OF THE TOV DURING TURN-OFF TRANSIENT PROCESS

To make an understandable analysis of the JTM indicator, the characterization behavior of the TOV during turn-off transient process is elaborated in this section.

Fig. 1 depicts the turn-off transient process of the IGBT module (Infineon FF50R12RT4), in which u_{ce}, i_{ce}, u_{ge}, $V_{G(ON)}$, $V_{G(OFF)}$, V_{pl}, V_{th}, V_{dc}, V_{cep}, and I_L are the TOV, the turn-off current, the gate voltage, the high level of drive voltage, the low level of drive voltage, the plateau voltage, the threshold voltage, the bus voltage, the peak voltage, and the load current, respectively. The parameters of the studied IGBT module are listed in Table I. As shown in Fig. 1, the turn-off process of the IGBT module is divided into three stages, i.e., the S1 stage, the S2 stage, and the S3 stage. Accordingly, the TOV is fully characterized in the three stages as follows.

S1 [t_0-t_1]: The switching signal of the IGBT module is changed from 1 to 0, and then the drive voltage is varied from $V_{G(ON)}$ to $V_{G(OFF)}$. Meanwhile, the interelectrode capacitors, i.e., C_{ge} and C_{cg}, discharge to the drive circuit due to the decrease of the drive voltage. As a result, the gate voltage u_{ge} is gradually decreased. Notably, the IGBT module is still in the saturation region during S1 stage, and hence the TOV and the turn-off current are maintained without obvious variations.

S2 [t_1-t_2]: The IGBT module is in the active region during S2 stage, and the gate voltage u_{ge} is clamped at the plateau voltage V_{pl} (see Fig. 1). With this, there is almost no current flowing across the interelectrode capacitor C_{ge}, and the gate current i_g is provided by the charging current of the interelectrode capacitor C_{cg}. Consequently, the TOV rises during S2 stage. To clearly illustrate this phenomenon, an equivalent circuit of the IGBT module during S2 stage is provided, as shown in Fig. 2.
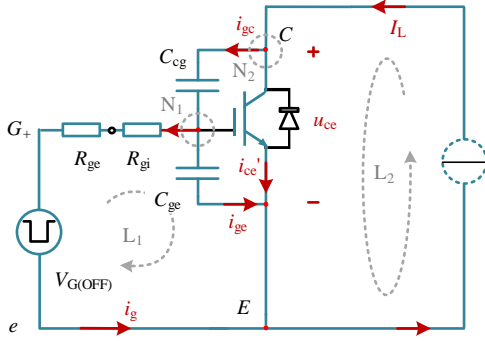
Fig. 2. Equivalent circuit of the IGBT module during S2 stage.

According to Fig. 2, with the Kirchhoff's voltage law (KVL), it can be obtained that

$$V_{G(OFF)} = -i_g \underbrace{(R_{ge} + R_{gi})}_{R_g} + u_{ge} \tag{1}$$

where i_g, R_{ge}, R_{gi}, and R_g are the gate current, the external gate resistance, the internal gate resistance, and the gate resistance, respectively. And, i_{ce}' can be expressed as [31]

$$i_{ce}' = \frac{K}{2}(u_{ge} - V_{th})^2 \tag{2}$$

with i_{ce}' and K being the steady-state value of the chip current and a gain that is related to the physical material of the IGBT module and affected by temperature. Taking the derivative of (2) gives

$$\frac{di_{ce}'}{dt} = K(u_{ge} - V_{th})\frac{du_{ge}}{dt} \tag{3}$$

In Fig. 2, according to the Kirchhoff's current law, the gate current i_g can be calculated as

$$\begin{aligned} i_g &= I_L - i_{ce}' - i_{ge} \\ &= I_L - \frac{K}{2}(u_{ge} - V_{th})^2 - C_{ge}\frac{du_{ge}}{dt} \end{aligned} \tag{4}$$

Substituting (2)-(4) to (1) yields

$$V_{G(OFF)} + I_L R_g = C_{ge} R_g \frac{du_{ge}}{dt} + \frac{K}{2}R_g(u_{ge} - V_{th})^2 + u_{ge} \tag{5}$$

According to the KVL, it can be further obtained that

$$u_{ce} = u_{ge} + V_{th} + \frac{1}{C_{cg}}\int[I_L - \frac{K}{2}(u_{ge} - V_{th})^2]dt \tag{6}$$

from which it seems that the temperature will make an obvious effect on K, V_{th}, and C_{cg} [31]. However, in the previous work, only the effects of temperature on K and V_{th} are concerned. Particularly, C_{cg} will also vary with temperature, and then affect the characterization behavior of the TOV during S2 stage, as elaborated as follows.

Fig. 3 shows the carrier conductive path of the IGBT module. As shown, the current flowing through the IGBT module is divided into the MOS channel current and the hole current. That is,

$$i_{ce} = i_{mos} + i_{pnp} \tag{7}$$

in which i_{ce}, i_{mos}, and i_{pnp} are the collector current, the MOS channel current, and the hole current, respectively.
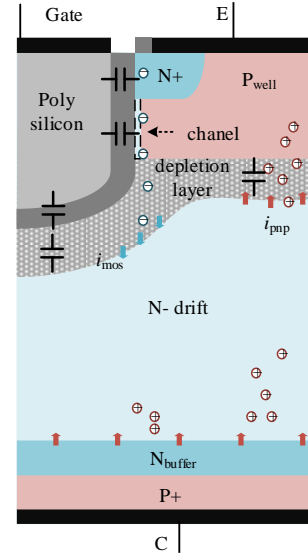

Fig. 3. Carrier conductive path of the IGBT module.

Ideally, the gate voltage u_{ge} is maintained as V_{pl} during S2 stage. This situation is different in practice. That is, the gate voltage u_{ge} experiences a small variation during S2 stage (see Fig. 1), and then i_{mos} is also decreased. Moreover, both the collector current i_{ce} and the hole current i_{pnp} are maintained during S2 stage. Referring to (7), the depletion layer of the base region expands, and hence a charge extraction current is produced to maintain i_{ce} (see Fig. 3). As a consequence, u_{ce} is increased during S2 stage. In all, it can be given by

$$\Delta i_{mos} = C_o \frac{du_{ce}}{dt} \tag{8}$$

where Δi_{mos} and C_o are defined as the deviation of the MOS channel current and the charge extraction capacitator, respectively. More specifically, C_o is used to describe the expanding speed of the depletion layer of the base region under the effects of Δi_{mos} [31]. And,

$$C_o = \frac{p_0}{N_T}[\alpha C_{dep} + (1-\alpha)C_{min}] \tag{9}$$

where p_0, N_T, C_{dep}, C_{min}, and α are the excess carrier density in the on-state at the anode p-n junction, the effective carrier density in the depletion region considering the carrier flow through the depletion region, the depletion layer capacitor, the depletion layer capacitor when the width of the depletion layer reaches the edge of the P+ region, and a gain that evaluates the contribution of C_{dep} for the charge extraction capacitator C_o, respectively. Considering the gate voltage u_{ge} is maintained as the plateau voltage V_{pl} during S2 stage, the gate current i_g can be rewritten as

$$i_g \approx C_{cg}\frac{du_{ce}}{dt} \tag{10}$$

With (8) and (10), the interelectrode capacitor C_{cg} can be deduced as

$$C_{cg} = \frac{i_g}{\Delta i_{mos}}C_o \tag{11}$$
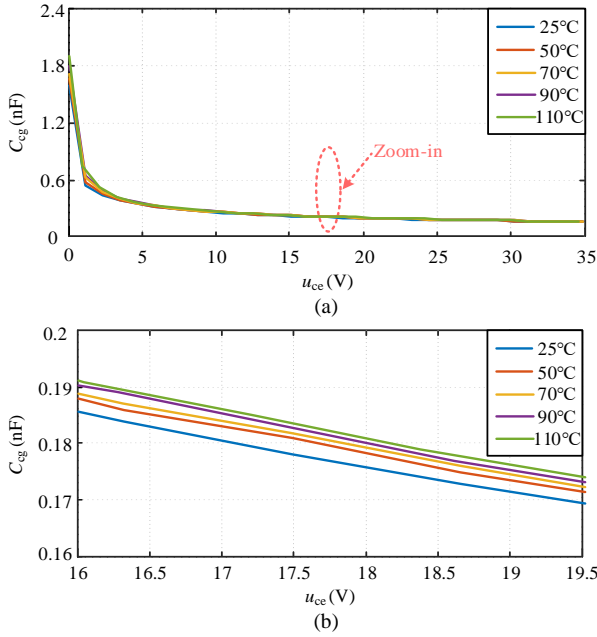
and i_g is calculated as

(a)

(b)

Fig. 4. Curves of the interelectrode capacitor C_{cg} with the increase of temperature: (a) the entire curves of the TOV and (b) the zoom-in area.
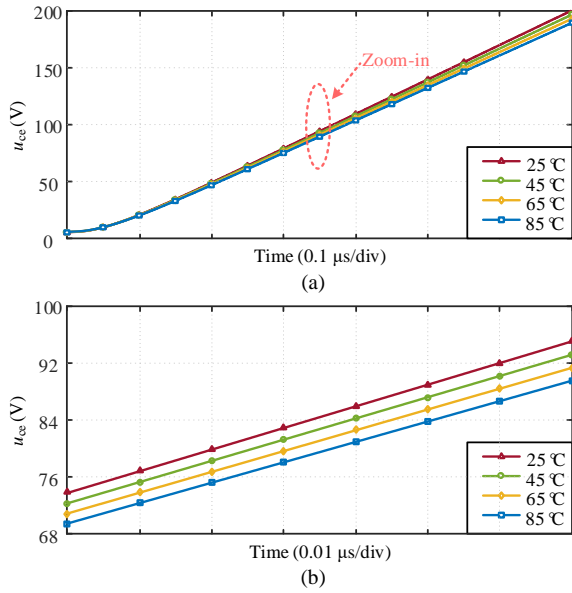

(a)

(b)

Fig. 5. Curves of the TOV with the increase of temperature during S2 stage: (a) the entire curves of the TOV and (b) the zoom-in area.

$$i_g = \frac{V_{pl} - V_{G(OFF)}}{R_g} \tag{12}$$

Supposing u_{ce} experiences a small variation, it is known that [31]

$$\Delta i_{mos} = K_p (u_{ge} - V_{th}) \Delta u_{ge} \tag{13}$$

with K_p and Δu_{ce} being the gain of the MOS channel and the deviation of u_{ce}, respectively. Substituting (12) and (13) into (11) entails

$$C_{cg} = \frac{(V_{pl} - V_{G(OFF)}) C_o}{R_g K_p (u_{ge} - V_{th}) \Delta u_{ge}} \approx \frac{(V_{pl} - V_{G(OFF)}) C_o}{R_g K_p (V_{pl} - V_{th}) \Delta u_{ge}} \tag{14}$$

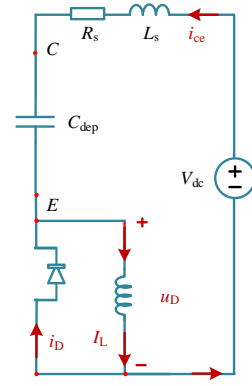It is suggested from (14) that C_{cg} will vary with temperature.

Fig. 6. Equivalent circuit of the IGBT module during S3 stage.

(a)

(b)
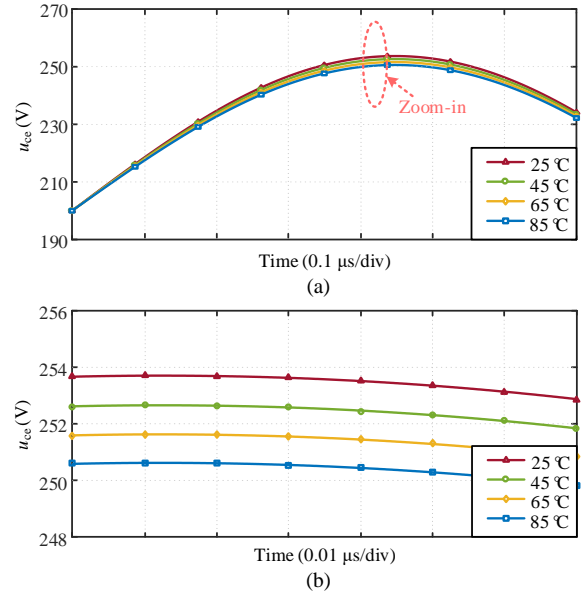
Fig. 7. Curves of the TOV with the increase of temperature during S3 stage: (a) the entire curves of the TOV and (b) the zoom-in area.

To verify the above discussion, experimental tests are performed by using a power analyzer (Agilent B1505A), and the results can be seen in Fig. 4. In this case, the interelectrode capacitor C_{cg} is tested with different temperature. The results in Fig. 4 show that the value of C_{cg} is increased with the increase of temperature, which verifies the above discussion.

Eventually, the curves of the TOV with the increase of temperature are depicted in Fig. 5. From Fig. 5, it is suggested that during S2 stage, with the increase of temperature, the time of the TOV to reach the bus voltage is increased but the slope of the TOV is decreased.

S3 [t_2-t_4]: The TOV of the IGBT module is increased to the bus voltage V_{dc}, and the freewheeling diode is turned on. Due to this, the load current is significantly decreased during S3 stage.

Similarly, an equivalent circuit of the IGBT module during S3 stage is presented in Fig. 6. As shown, R_s, L_s, and u_D are the equivalent resistance, the equivalent inductance, and the negative value of the forward voltage of the diode, respectively. From Fig. 6, it can be deduced as

Fig. 8. Effects of the bond wire aging on the TOV during turn-off transient.

Fig. 9. Effects of the load current on the TOV during turn-off transient.

$$u_{ce} + L_s \frac{di_{ce}}{dt} + R_s i_{ce} = V_{dc} \qquad (15)$$

with,

$$i_{ce} = C_{dep} \frac{du_{ce}}{dt} \qquad (16)$$

Subsequently, it can be given by

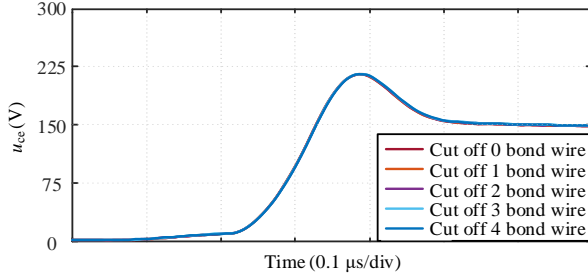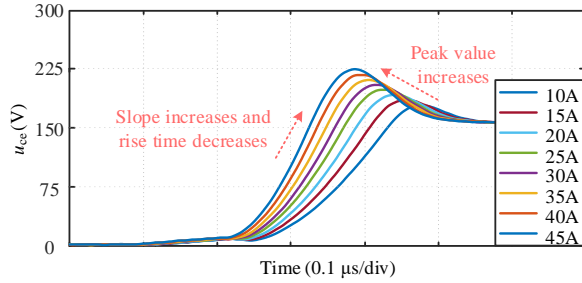$$V_{dc} = C_{dep} L_s \frac{d^2 u_{ce}}{dt^2} + C_{dep} R_s \frac{du_{ce}}{dt} + u_{ce} \qquad (17)$$

According to the above analysis, the curves of the TOV with the increase of temperature during S3 stage are illustrated in Fig. 7, in which the test cases are identical to those in Fig. 5. Clearly, the peak value of the TOV is decreased with the increase of temperature during S3 stage.

III. PARAMETER DEPENDENCE ANALYSIS OF THE TOV

As discussed previously, in many TSEP-based JTM methods, the junction temperature indicators are troubled by various disturbances, and hence a compromised accuracy of the JTM method is obtained. With this consideration, in this section, a detailed parameter dependence analysis of the TOV is accordingly provided.

A. Effects of Bond Wire Aging on the TOV

The effects of bond wire aging on the TOV are first investigated, which is shown in Fig. 8. In this case, the bus voltage, the junction temperature, and the load current are set to 150 V, 70°C, and 45 A, respectively. The bond wire aging is emulated by artificially cutting off the bonding wire. Observations in Fig. 8 indicate that the curves of the TOV with different cut-off bond wires are roughly same, implying that the bond wire aging makes a negligible effect on the behavior of the TOV.
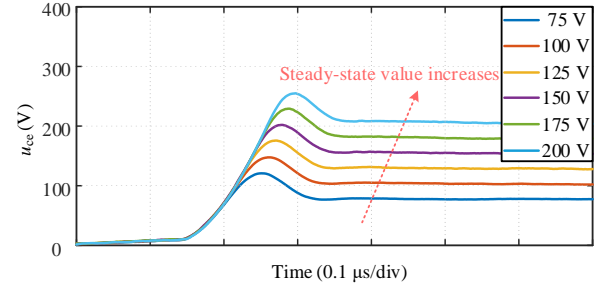

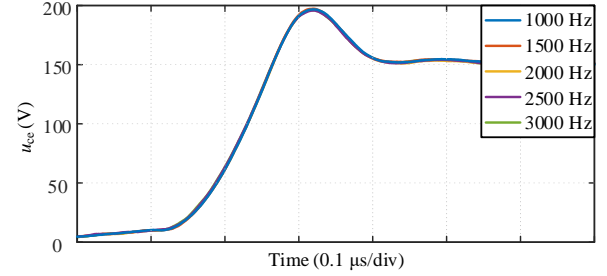Fig. 10. Effects of the bus voltage on the TOV during turn-off transient.

Fig. 11. Effects of the switching frequency on the TOV during turn-off transient process.

B. Effects of Load Current on the TOV

Then, the effects of load currents on the TOV are further investigated, and the corresponding test results are shown in Fig. 9. In this case, the bus voltage and the junction temperature are set to 150 V and 70°C, respectively. It is clear from Fig. 9 that with the increase of the load current, the slope of the TOV is increased, and the rise time of the TOV is decreased during S2 stage. Meanwhile, the peak value of the TOV during S3 stage is increased. The results in Fig. 9 demonstrate that the TOV is accompanied by the challenge of load current dependence, which may hinder the applicability of the proposed JTM method.

C. Effects of Bus Voltage on the TOV

The effects of bus voltage on the TOV are focused on, and the corresponding experimental tests are performed. Fig. 10 illustrates the performance of the TOV with different bus voltage, in which the junction temperature and the load current are set to 20°C and 20 A, respectively. Clearly, the TOV with various bus voltage exhibits different behaviors, which leads to the conclusion that the variations of the bus voltage will obviously affect the performance of the TOV. In spite of this, generally, the bus voltage in the single-phase PWM rectifier approaches a constant value [32]-[34]. With this consideration, the effects of the bus voltage on the behavior of the TOV may be neglected.

D. Effects of Switching Frequency on the TOV

The performance of the TOV with different switching frequencies is experimentally explored, which can be seen in Fig. 11. In this case, the bus voltage, the junction temperature, and the load current are set to 150 V, 50°C, and 20 A, respectively. Seen from Fig. 10, it is indicated that the TOV shows a similar behavior with different switching frequencies. That means, the effects of switching frequency on the behavior of the TOV are negligible.
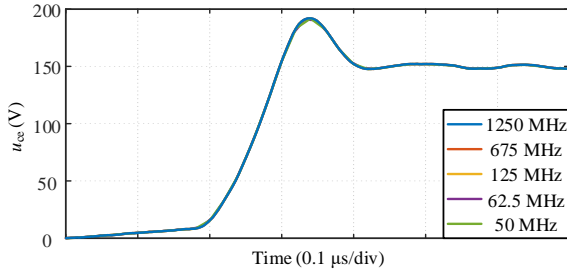
Fig. 12. Effects of the sampling frequency on the TOV during turn-off transient.
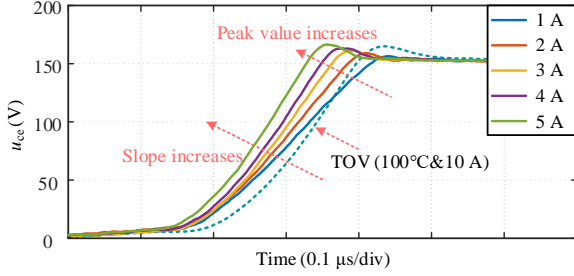

Fig. 13. Effects of a low junction temperature with different low load currents on the TOV during turn-off transient.
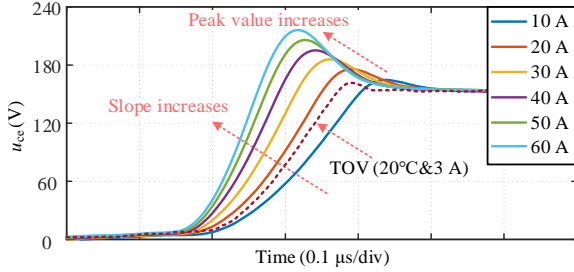

Fig. 14. Effects of a high junction temperature with different high load currents on the TOV during turn-off transient.

E. Effects of Sampling Frequency on the TOV

A performance analysis of the TOV with different sampling frequencies is conducted, and the results are presented in Fig. 12. In the experimental tests, the sampling frequency is originally set to 1250 MHz. To further examine the effects of the sampling frequency on the behavior of the TOV, the corresponding experimental tests are carried out, and the bus voltage, the junction temperature, and the load current in this case are set to 150 V, 30°C, and 15 A, respectively. Results in Fig. 12 suggest that an inconspicuous difference can be observed in the TOV with different sampling frequencies, which indicates that the sampling frequency will not obviously affect the TOV.

F. Effects of a Small Load Current and a Low Junction Temperature on the TOV

The behavior of the TOV at a small load current and a low junction temperature is investigated through experimental tests, and the results are presented in Fig. 13. Seen from Fig. 13, the junction temperature and the bus voltage are set to 20°C and 150 V, respectively. According to the results, it is known that the increase of the load current (from 1 A to 5 A) makes the curves of the TOV shift to the left. More specifically, both the slope of the TOV and the peak value of the TOV are obviously increased.
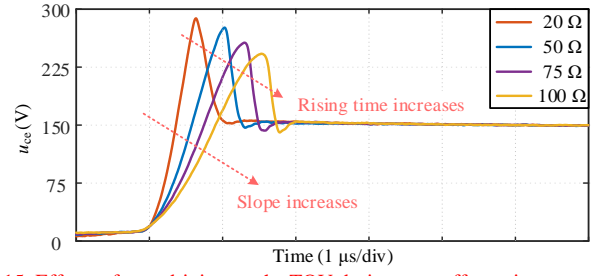

Fig. 15. Effects of gate driving on the TOV during turn-off transient.

G. Effects of a High Load Current and a High Junction Temperature on the TOV

The effects of a high load current and a high junction temperature on the TOV are investigated, which can be seen in Fig. 14. As shown in Fig. 14, the junction temperature and the bus voltage are set to 100°C and 150 V. Similarly, with the increase of the load current (from 10 A to 50 A), the curves of the TOV shift to the left, and both the peak values and the slopes of the TOV are increased.

Moreover, the performance of the TOV at a low junction temperature and a small load current is compared to that at a high load current and a high junction temperature. It is suggested from Figs. 13 and 14 that that an IGBT turns off slowly at a small load current or a high junction temperature, where the load current and the junction temperature affect the TOV inversely. Despite this, the effects of the small load current and the high junction temperature on the behaviors of the TOV is essentially different. That is, with the decrease of the load current, the extended speed of the depletion layer becomes slow and the electron hole pairs are deduced. As a consequence, the IGBT modules turn off slowly. Meanwhile, the small load current may lead to the small overshoot of the TOV with the effects of parasitic inductance of the IGBT modules. By comparison, the high junction temperature results in an increased lifetime of the depletion layer carrier, which slows down the decay rate of carrier recombination. By doing so, the turn-off time is accordingly increased.

With the above analysis, though both the small load current and the high junction temperature make the IGBT modules turn off slowly, their function mechanisms are different, and accordingly the characterization behaviors of the TOV are also different. Due to this, there is a difference in the feature information of the TOV under the two cases (see the dash lines of Figs. 13 and 14). With the excellent feature recognition capability of the CNN, the task of accurate junction temperature monitoring can be accomplished.

H. Effects of Gate Driving on the TOV

Finally, the effects of gate driving on the TOV are investigated, which can be seen in Fig. 15. As shown in Fig. 15, the junction temperature, the load current, and the bus voltage are set to 20°C, 60 A, and 150 V. And, the gate resistance variations are developed to emulate the active gate driver. It is concluded from Fig. 15 that, as expected, the increased gate resistance leads to the increase of the rise time and the increase of the slope (more analysis results can be seen in Section II).
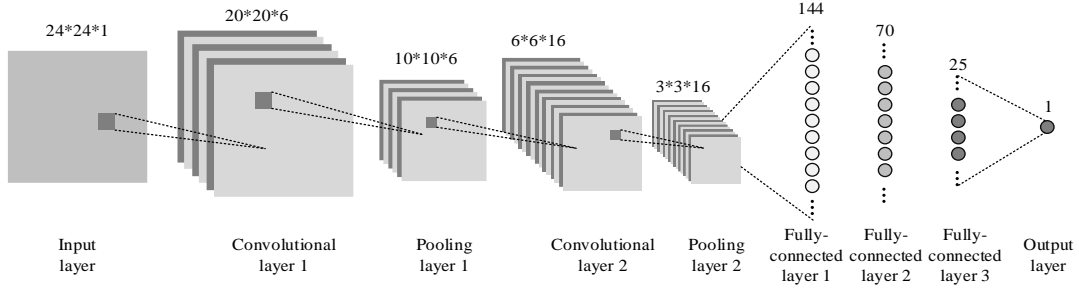
Fig. 16. Structure of the CNN in the proposed JTM method.

That means, the active gate driver may cause different behaviors of the TOV, and affect the performance of the proposed JTM method. Hence, further efforts should be implemented when being applied in the IGBT module with active gate driver.

IV. FEATURE INFORMATION EXTRACTION METHOD OF THE TOV BASED ON CONVOLUTIONAL NEURAL NETWORKS

In Section III, it is revealed from the analysis that the performance of the proposed JTM method may be degraded with different load currents. In this section, a viable solution to this problem is developed by using the CNN, in which the information of the load current is not required.

A. Basics of the CNN

The CNN is one of the representatives of the deep learning algorithms, which can be regarded as a class of feedforward neural networks that include convolutional computation and have a deep structure. Distinctive features like excellent global and local feature recognition capability are directing considerable attention to the CNN [35], [36].

The structure of the CNN in the proposed JTM method is shown in Fig. 15, which includes nine layers, i.e., the input layer, the convolutional layer, the pooling layer, the fully connected layer, and the output layer. It is worth noting that the number in Fig. 15 means the size of the sample, i.e., a 3-dimensional (3D) array with width, height, and length. The details of the CNN will be discussed in the following sections.

B. Convolutional Layer of the CNN

The convolutional layer is critical for the CNN, which is used to perform feature extraction from the input layer (generally, the input of the CNN is a 2D or 3D data matrix). Then, the extracted features are mapped to form new feature. The convolutional layer has a series of convolutional kernels, and every convolutional kernel convolves with the input data matrix to produce the convolved feature. An example of the 2D convolution is shown in Fig. 17. As shown, a 2×2 convolutional kernel is aligned on the upper left of the 4×4 input data matrix, and then slides to the right in turn. It is worth noting from Fig. 17 that each slide step gives an output.

The parameters of the convolutional kernel, i.e., the size of the convolutional kernel, the stride, and the padding, make an obvious effect on the feature extraction performance. Notably, a CNN with a small size of the convolutional kernel may be susceptible to the loss of feature information.
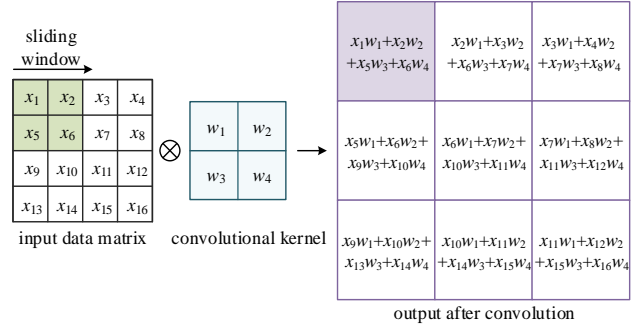
Fig. 17. An example of the 2D convolution.
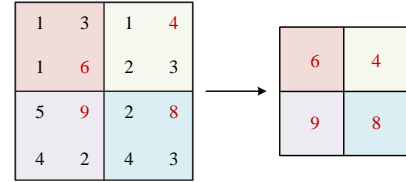
Fig. 18. An example of the max pooling.

While, the large size of the convolutional kernel may bring the concern of computational burden. Additionally, the stride is adopted to reduce the size of the input data matrix and the computational burden. Moreover, the padding is used to maintain the spatial size of the output data matrix. The size of the output data matrix is calculated as

$$\begin{cases} W_o = \dfrac{W_i + 2P - F}{S} + 1 \\ H_o = \dfrac{H_i + 2P - F}{S} + 1 \\ L_o = N \end{cases} \quad (18)$$

in which W_i, H_i, L_i, W_o, H_o, L_o, P, F, S, and N are the width, height, and length of the input data matrix, the width, height, and length of the output data matrix, the number of the padding, the size of the convolutional kernel, the stride, and the number of the convolutional kernel, respectively. When S is set to 1, P becomes $(F-1)/2$. With this, the width and height of the input data matrix are equal to that of the output data matrix [35], [36].

C. Pooling Layer of the CNN

After feature extraction in the convolutional layer, the extracted feature is further processed in the pooling layer for feature selection and information filtering, which is helpful for reducing the size of the data and avoiding the issue of overfitting.

Fig. 19. Flowchart of the proposed feature extraction method based on the CNN.

There are several pooling methods in the CNN, e.g., the max pooling, the mean pooling, the stochastic pooling, and the spectral pooling. In this paper, the max pooling method is used due to its easy implementation. Fig. 18 shows an example of the max pooling. Seen from Fig. 18, the extracted feature is divided into four 2×2 regions. The maximum value in the 2×2 region is extracted and the rest data are discarded. By doing so, the target of data dimensionality reduction is easily achieved.

D. Fully Connected Layer of the CNN

The fully connected layer is the last part of the CNN, which performs the combination of the extracted features from the convolutional layer and the pooling layer for the purpose of classification or prediction. More specifically, in the fully connected layer, every node is fully interconnected with the nodes of the previous layer. And, the extracted feature from the previous layer is integrated and mapped to the sample label space. Then, a weighted summation method is carried out for the extracted feature, and finally completes the task of classification or prediction.
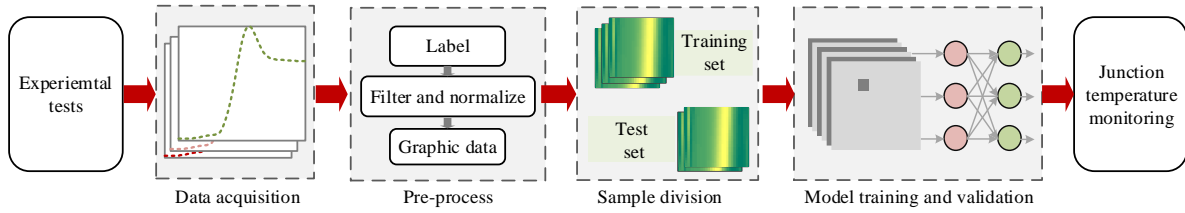
E. Proposed Feature Extraction Method Based on the CNN

In the proposed JTM method, the full TOV waveform is regarded as the inputs, and the interval sampling method is adopted to obtain the data of the TOV. Then, with the excellent global and local feature recognition capability of the CNN, the feature information of the TOV is selected and fused. It is worth noticing that the feature information of the TOV is the information of the TOV that is independent on the load current and highly related to the junction temperature. Fig. 19 illustrates the flowchart of the proposed feature extraction method based on the CNN, and this feature extraction method is accomplished in four recursive steps, i.e., the data acquisition, the pre-process, the sample division, and the model training and validation. First of all, after executing considerable experimental tests, adequate data of the TOV considering different cases, e.g., different junction temperature, different load currents, and different aging degrees of bond wire, are collected. Next, the collected data are labeled with the information of junction temperature, and the labeled data of the TOV are filtered and normalized to guarantee the performance of the model training. The processed data of the TOV are further converted into the graphic data (an array only with width and height) in a parallel arrangement. Then, these graphic data are divided into two groups, i.e., the training set and the test set. The training set is used to train the model, and the accuracy of the training model is examined by the test set. Finally, the task of JTM for the IGBT module is implemented with the well-trained model.
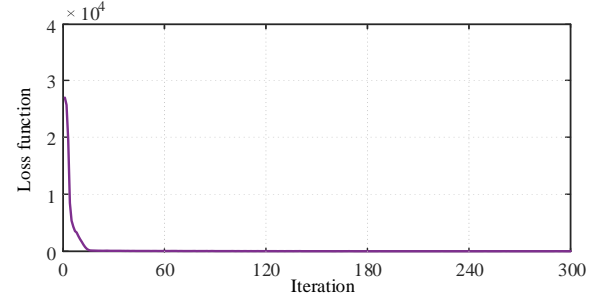
Fig. 20. Curve of the loss function in the double-pulse tests.
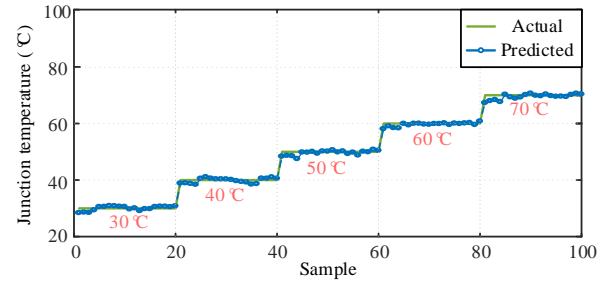
Fig. 21. Performance of the proposed JTM method according to the double-pulse tests.
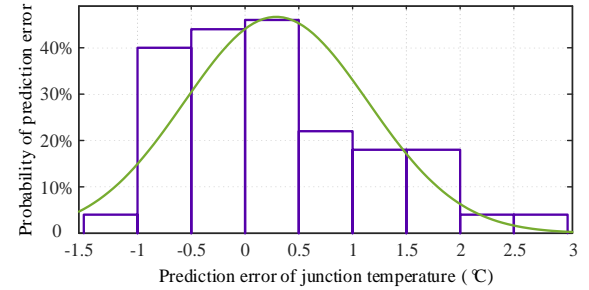
Fig. 22. Prediction error distribution of the proposed JTM method according to the double-pulse tests.

As mentioned previously, in the convolutional layer, the convolution kernels are used to extract the feature information of the TOV. Heightened attention should be paid to the convolution kernels. That is, when the data of the TOV with the same label under different load currents appear in the input layer, the weight coefficients of the convolution kernel are accordingly adjusted. By doing so, the effects of load currents on the feature information of the TOV are effectively mitigated. Then, the employment of the pooling layer eliminates the redundant information of the local feature. Afterward, the extracted feature information that avoids load current dependence is fused through the fully connected layer. With the assistance of the CNN, the concern of load current dependence is addressed well, further ensuring the performance of the proposed JTM method.

V. DOUBLE-PULSE TEST VERIFICATION

The double-pulse tests are first executed for verification purposes. In the double-pulse tests, there are 200 test samples of the TOV from the double-pulse tests. Then, the collected samples are divided into the training set and the test set with the ratio of 1:1. To perform a satisfactory training performance, the iteration and the batch size are set to 300 and 10, respectively. Moreover, the minimum mean square error function is selected as the loss function to evaluate the performance of the training model.

Fig. 20 presents the loss function during training process. As shown, in the beginning, the value of the loss function is tremendous. After 20 iterations, the value of the loss function is dramatically decreased and approaches to 0, which confirms that a proper training performance is achieved by the CNN. Then, the well-trained model of the CNN is adopted in the test set to perform junction temperature prediction, and the results are shown in Figs. 21 and 22, respectively. The results in Figs. 21 and 22 show that the predicted junction temperature from the proposed JTM method makes a good agreement with the actual junction temperature, and the prediction error lies in a reasonable range (within ±3°C). That is, the double-pulse test results show that the proposed JTM method features a satisfactory performance.

VI. EXPERIMENTAL TEST VERIFICATION

A. Experimental Test Bench

The experimental tests are conducted on the test bench of a single-phase PWM rectifier to further investigate the performance of the proposed JTM method. The block diagram and the photo of the experimental test bench are shown in Figs. 23 and 24, respectively. As shown, the test bench consists of three parts, i.e., the main circuit, the controller, and the junction te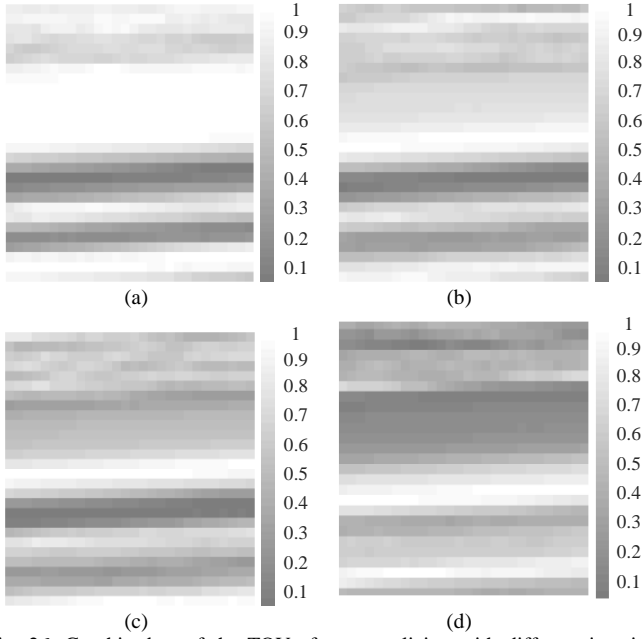mperature monitoring circuit. In the main circuit, the single-phase PWM rectifier is fed by a programmable AC power supply (Chroma 61511). The DC-link support capacitor C_d, a filtering inductance L_f and a filtering capacitor C_f are employed as the role of realizing energy storage and filtering, respectively. And, the control strategy of the single-phase PWM rectifier is implemented on a dSPACE 1006 platform. As for the junction temperature monitoring circuit, it includes a heating plate and an infrared thermometer. The heating plate is responsible for heating the IGBT module, and the infrared thermometer provides the actual junction temperature of the tested IGBT module. Additionally, the parameters of the experimental test bench are listed in Table II.

B. Experimental Data Acquisition and Conversion

In the experimental tests, different cases including different junction temperature and different load currents are considered. The results in Fig. 25 shows that with the increase of junction temperature, the rise time of the TOV is increased, and yet the peak value of the TOV is decreased during turn-off transient process. This agrees with the above analysis in Section III.

Fig. 23. Block diagram of the experimental test bench.

Fig. 24. Photo of the experimental test bench.

TABLE II
PARAMETERS OF THE EXPERIMENTAL TEST BENCH

Parameter	Value	Parameter	Value
Fundamental frequency (Hz)	50	Filtering inductance L_f (mH)	3.4
AC-side inductance L_s (mH)	3.4	Filtering capacitor C_f (μF)	1500
DC-link capacitor C_d (μF)	3000	Load resistance (Ω)	33

Fig. 25. Data of the TOV with different temperature and different load currents: (a) the training set and (b) the test set.

As mentioned previously, it is necessary to convert the labeled data into the graphic data (see Fig. 19). Fig. 26 illustrates the graphic data after normalizing with different junction temperature, in which the number represents the gray coefficient. Seen from Fig. 26, it can be concluded that the graphic data of the TOV with different junction temperature present different feature information.

Fig. 26. Graphic data of the TOV after normalizing with different junction temperature: (a) 35℃, (b) 45℃, (c) 55℃, and (d) 70℃.
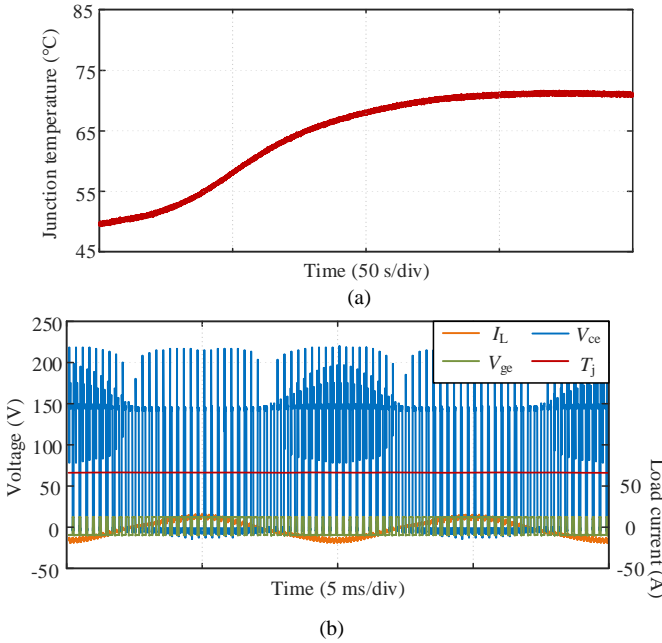

Fig. 27. Curve of the junction temperature with time: (a) the whole curve of the junction temperature with time and (b) the curve of the junction temperature with time and load current at steady state.

C. Curve of the Junction Temperature with Time

The curve of the junction temperature with time by using the experimental tests is illustrated in Fig. 27. As shown, the junction temperature of the IGBT module is increased first, and then approaches a steady-state value (see Fig. 27(a)). When the single-phase PWM rectifier is operated under normal conditions, the junction temperature is barely varied at steady state (see the red line in Fig. 27(b)).
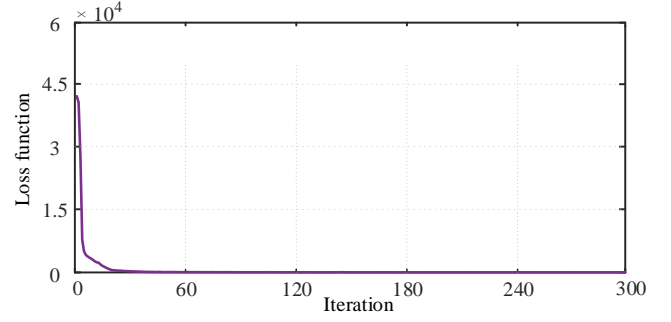
Fig. 28. Curve of the loss function in the experimental tests.
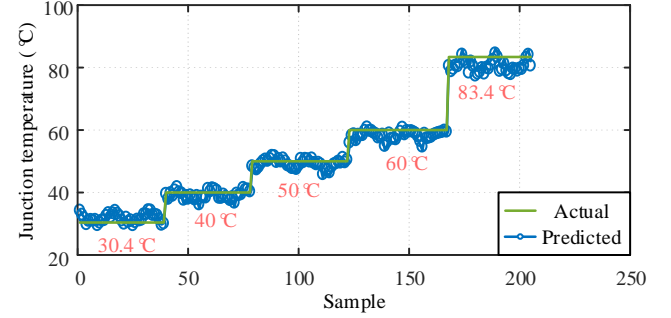

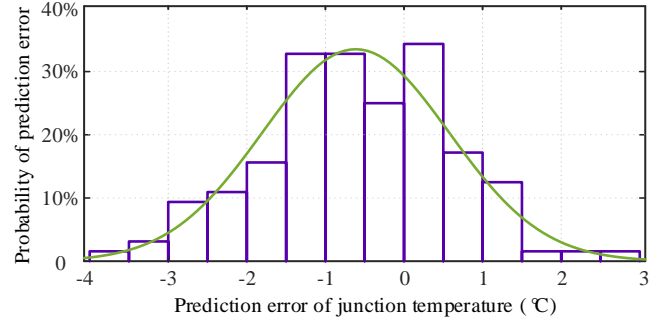Fig. 29. Performance of the proposed JTM method according to the experimental tests.

Fig. 30. Prediction error distribution of the proposed JTM method according to the experimental tests.

D. Performance of the Proposed JTM Method

In the experimental tests, the iteration and the batch size are set to 300 and 10, respectively. And, the minimum mean square error function is also used as the loss function, which is depicted in Fig. 28. According to the results in Fig. 28, the value of the loss function approaches 0 after 20 iterations, and remains in a small range, which indicates that the CNN makes an achievement in terms of good training performance. Then, the well-trained model is used for junction temperature prediction, and the results are shown in Figs. 29 and 30, respectively. According to the results in Figs. 29 and 30, it is reasonable to say that an acceptable junction temperature prediction is obtained by the proposed JTM method, and the prediction error remains limited in a narrow range of ±5℃ under this case. Notably, in Fig. 29, the data of 30.4℃ and 83.4℃ are not included in the training set. Despite this, the proposed JTM method shows a satisfactory performance. That means, the proposed JTM method predicts the junction temperature accurately when the data of the test set differ from those of the training set.
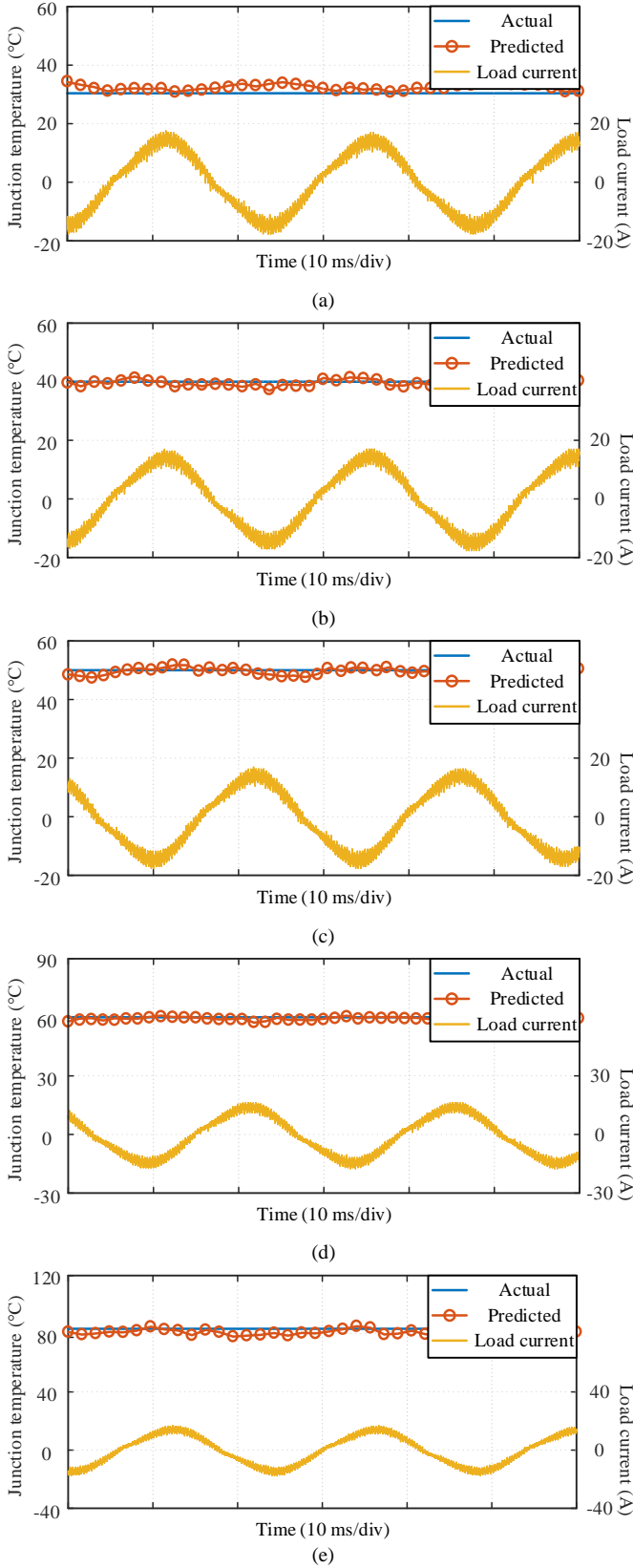
Fig. 31. Performance of the proposed JTM method at different junction temperature with time: (a) 30.4°C, (b) 40°C, (c) 50°C, (d) 60°C, and (e) 83.4°C.
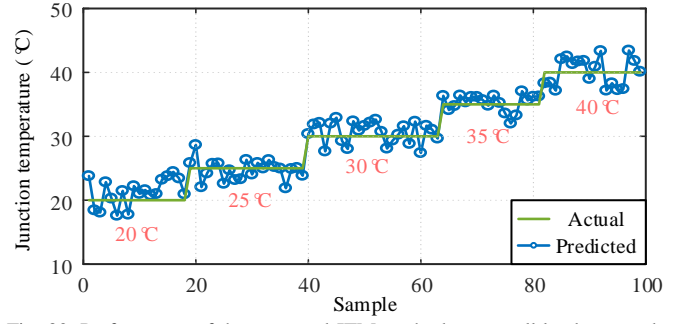

Fig. 32. Performance of the proposed JTM method at a small load current but a low junction temperature.
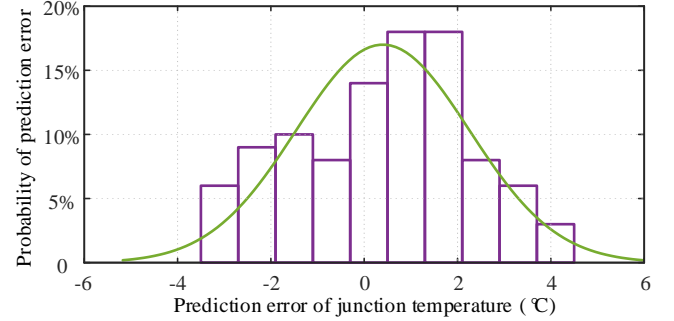

Fig. 33. Prediction error distribution of the proposed JTM method at a small load current but a low junction temperature.
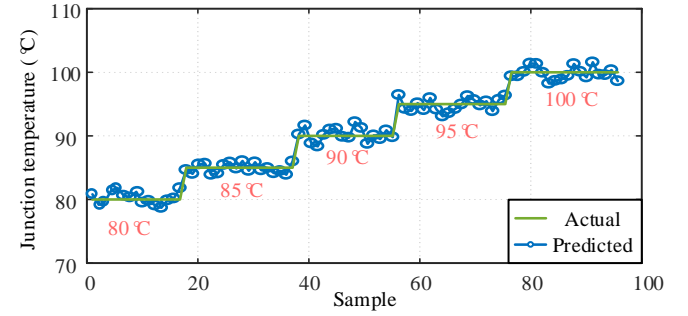

Fig. 34. Performance of the proposed JTM method at a high load current but a high junction temperature.
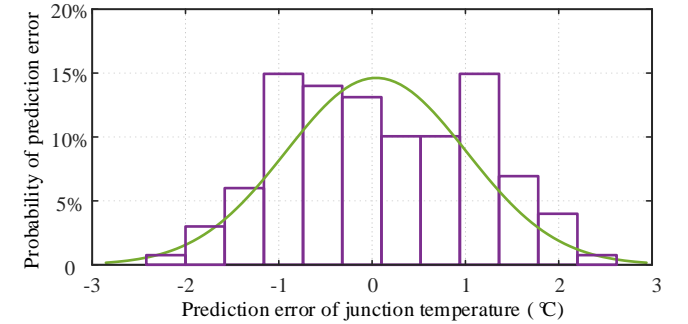

Fig. 35. Prediction error distribution of the proposed JTM method at a high load current but a high junction temperature.

Furthermore, the performance of the proposed JTM method at different junction temperature with time is shown in Fig. 31. The experimental results in Fig. 31 indicate that the proposed JTM method behaves well when working at different junction temperature with time.
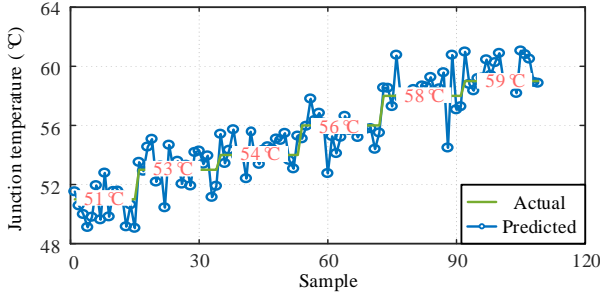
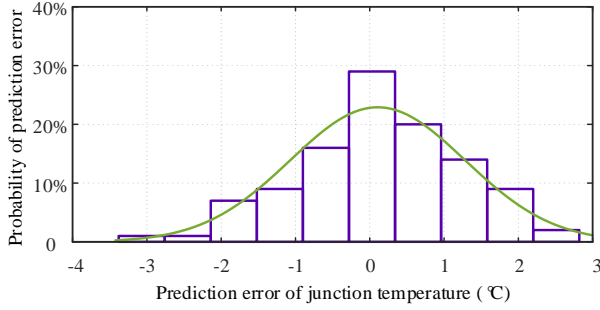Fig. 36. Performance of the proposed JTM method with a limited resolution.

Fig. 37. Prediction error distribution of the proposed JTM method with a limited resolution.

E. Performance of the Proposed JTM Method at a Small Load Current but a Low Junction Temperature

Figs. 32 and 33 shows the performance of the proposed JTM method at a small load current but a low junction temperature. In this case, the junction temperature is varied from 20°C to 40°C, and the variations of the load current from 1 A to 5 A are applied. According to the results in Figs. 32 and 33, it can be seen that the proposed JTM method provides a roughly good performance in terms of junction temperature prediction, and the prediction error lies in the range of ±6°C. As mentioned previously, the different behaviors of the TOV at a small load current but a low junction temperature lead to the different feature information of the TOV. With the assistance of the CNN, the performance of the proposed JTM method at a small load current but a low junction temperature is ensured.

F. Performance of the Proposed JTM Method at a High Load Current but a High Junction Temperature

Meanwhile, to further evaluate the performance of the proposed JTM method, the case of a high load current but a high junction temperature is conducted, which is shown in Figs. 34 and 35. In this case, the junction temperature and the load current are varied from 80°C to 100°C, and from 15 A to 20 A (the maximum operating current in the test bench of the single-phase PWM rectifier), respectively. Seen from Figs. 34 and 35, the performance of the proposed JTM method at a high load current but a high junction temperature is acceptable, and the junction temperature prediction error is within a reasonable range of ±3°C, which should be attributable to the obvious difference of the TOV at a high load current but a high junction temperature. Due to this, the CNN has the ability of accurately extracting the feature information of the TOV in this case.
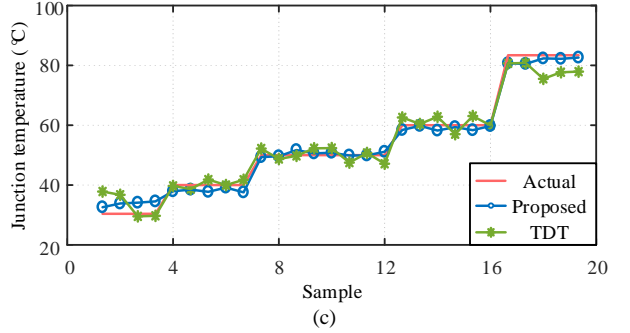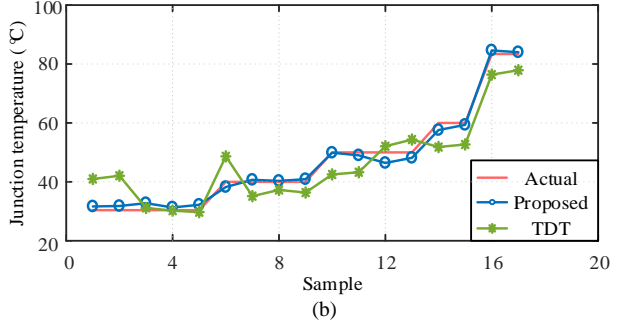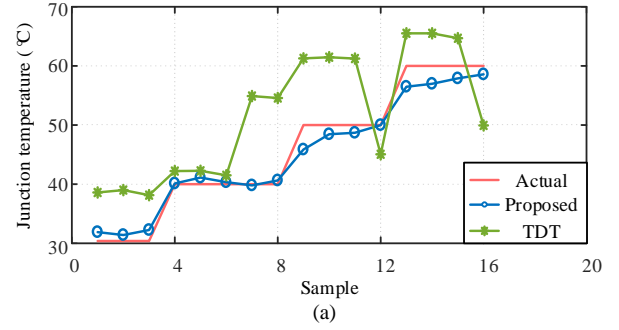

(a)

(b)

(c)

Fig. 38. Performance comparison between the proposed JTM method and the TDT method with different load currents: (a) the load current of 5 A, (b) the load current of 10 A, and (c) the load current of 15 A.

TABLE III
PERFORMANCE COMPARISON UNDER DIFFERENT LOAD CURRENTS IN TERMS OF MAXIMUM PREDICTION ERROR

Method	Load current of 5 A (°C)	Load current of 10 A (°C)	Load current of 15 A (°C)
Proposed	-4.91	-3.59	4.15
TDT	15.11	11.68	-7.88

TABLE IV
PERFORMANCE COMPARISON UNDER DIFFERENT LOAD CURRENTS IN TERMS OF MINIMUM PREDICTION ERROR

Method	Load current of 5 A (°C)	Load current of 10 A (°C)	Load current of 15 A (°C)
Proposed	0.12	0.10	-0.07
TDT	1.51	-0.17	0.74

TABLE V
PERFORMANCE COMPARISON UNDER DIFFERENT LOAD CURRENTS IN TERMS OF MEAN PREDICTION ERROR

Method	Load current of 5 A (°C)	Load current of 10 A (°C)	Load current of 15 A (°C)
Proposed	0.92	0.51	0.26
TDT	5.79	3.43	1.55

G. Performance of the Proposed JTM Method with a Limited Resolution

The dependency of resolutions is an aspect to be addressed in the proposed JTM method. With this, the experimental test with a limited resolution is performed, and the results are shown in Figs. 36 and 37. In this case, the junction temperature is increased from 51℃ to 59℃. The results in Figs. 36 and 37 show that with a limited resolution, the training performance of the CNN is maintained, and hence the junction temperature prediction error is limited in a proper range of ±4℃. In spite of this, the limited resolution adversely affects the performance of the proposed JTM method. That is, with a limited resolution, the obvious ripples appear in the predicted junction temperature, which makes the accurate distinguish of the actual junction temperature become tough (see Fig. 36). Considering this, further research efforts should be made to guarantee the performance of the proposed JTM method with a limited resolution.

H. Performance Comparison Between the Proposed JTM Method and the TDT Method

As discussed before, the load current dependence is a troublesome problem that may lead to a compromised accuracy of junction temperature prediction. Therefore, the effects of the load current are experimentally explored for the proposed JTM method. Moreover, the performance of the proposed JTM method with different load currents is compared to that of the turn-off dead time-based JTM method [22] (hereafter, referred as to the TDT method), which is shown in Fig. 38. As shown in Fig. 38, there is a noticeable difference in the performance of the TDT method with different load currents. More specifically, the TDT method provides a good junction temperature prediction performance with the load current of 15 A. However, the TDT method behaves unsatisfactorily with the load currents of 5 A and 10 A, and a large prediction error can be observed in the TDT method. The experimental results also lead to the conclusion that the TDT method is unable to deal with the knotty problem of load current dependence. By comparison, the proposed JTM method makes an apparent improvement. That is, a satisfactory performance with different load currents is obtained by implementing the proposed JTM method. Meanwhile, the improvement of the proposed JTM method justifies the efforts of using the CNN that goes toward the solution of load current dependence. Moreover, comparable results between the proposed JTM method and the TDT method with different load currents are respectively concluded in Table III, Table IV, and Table V, which clearly illustrates that the proposed JTM method features a better performance.

VII. CONCLUSION

The accurate junction temperature monitoring is highly helpful for reliability evaluation and health management of IGBT modules. However, this task becomes tough due to the troublesome problem of load current dependence. To address this, a JTM method based on the TOV and CNN was proposed in this paper for IGBT modules. In the proposed JTM method,

the characterization behavior of the TOV during turn-off transient process was analyzed in detailed. Then, a parameter dependence analysis of the TOV was performed. It is clear from the analysis that the availability of the proposed JTM method may be degraded with the problem of load current dependence. Accordingly, an innovative solution, i.e., using the CNN, was developed to ensure the performance of the proposed JTM method, in which the information of the load current is not required. The effectiveness of the proposed JTM method under different operating conditions was validated by extensive double-pulse tests and experimental tests based on the test bench of a single-phase PWM rectifier, and compared with that of the TDT method. The experimental results point out that, the proposed JTM method is compelling for IGBT modules, and interesting benefits are achieved in terms of avoiding the problem of load current dependence.

Compared to the proven TSEP methods, with the assistance of the CNN, the full waveform of the TOV is used to implement the task of junction temperature monitoring, which enables to deal with the issue of the complex measurement of the TSEP. Additionally, benefiting from the excellent global and local feature recognition capability of the CNN, the proposed JTM method may provide accurate junction temperature estimation with the similar behavior of the TOV under different cases (e.g., a low junction temperature and a small load current, and a high junction temperature and a high load current). However, the proposed JTM method is not a final solution to the JTM of the IGBT module. This is because that the limited resolution may lead to an unacceptable performance of junction temperature monitoring. Therefore, further research efforts must be developed to improve the industrial applicability.

REFERENCES

[1] J. Zhang, J. Liu, S. Zhong, J. Yang, N. Zhao, and T. Q. Zheng, "A power electronic traction transformer configuration with low-voltage IGBTs for onboard traction application," *IEEE Trans. Power Electron.*, vol. 34, no. 9, pp. 8453-8467, Sep. 2019.

[2] C. Dincan, P. Kjaer, Y. H. Chen, S. Munk-Nielsen, and C. L. Bak, "Analysis of a high-power, resonant DC-DC converter for DC wind turbines," *IEEE Trans. Power Electron.*, vol. 33, no. 9, pp. 7438-7454, Sep. 2018.

[3] S. Yang, A. Bryant, P. Mawby, D. Xiang, L. Ran, and P. Tavner, "An industry-based survey of reliability in power electronic converters," *IEEE Trans. Ind. Appl.*, vol. 47, no. 3, pp. 1441-1451, May/Jun. 2011.

[4] H. Wang and F. Blaabjerg, "Power electronics reliability: State of the art and outlook," *IEEE J. Emerg. Sel. Top. Power Electron*, vol. 9, no. 6, pp. 6476-6493, Dec. 2021.

[5] A. Hanif, Y. Yu, D. DeVoto, and F. Khan, "A comprehensive review toward the state-of-the-art in failure and lifetime predictions of power electronic devices," *IEEE Trans. Power Electron.*, vol. 34, no. 5, pp. 4729-4746, May 2019.

[6] X. Xiao, X. Ge, Q. Ke, L. Yong, Y. Liao, H. Wang, and Y. Zhang, "An adaptive temperature observer for electrothermal analysis of IGBT based on temperature characteristics," *IEEE J. Emerg. Sel. Top. Power Electron.*, 2022, early access.

[7] Y. Zhang, X. Ge, Y. Zhang, D. Xie, B. Yao, and H. Wang, "A novel three-pulse equivalent power loss profile for simplified thermal estimation," *IEEE J. Emerg. Sel. Top. Power Electron.*, vol. 9, no. 6, pp. 6875-6885, Dec. 2021.

[8] L. Dupont, Y. Avenas, and P. Jeannin, "Comparison of junction temperature evaluations in a power IGBT module using an IR camera

and three thermosensitive electrical parameters," *IEEE Trans. Ind. Appl.*, vol. 49, no. 4, pp. 1599-1608, Jul./Aug. 2013.

[9] B. Ji, X. Song, W. Cao, V. Pickert, Y. Hu, J. W. Mackersie, and G. Pierce, "In situ diagnostics and prognostics of solder fatigue in IGBT modules for electric vehicle drives," *IEEE Trans. Power Electron.*, vol. 30, no. 3, pp. 1535-1543, Mar. 2015.

[10] A. S. Bahman, K. Ma, and F. Blaabjerg, "A lumped thermal model including thermal coupling and thermal boundary conditions for high-power IGBT modules," *IEEE Trans. Power Electron.*, vol. 33, no. 3, pp. 2518-2530, Mar. 2018.

[11] M. Ma, W. Guo, X. Yan, S. Yang, X. Zhang, W. Chen, and G. Cai, "A three-dimensional boundary-dependent compact thermal network model for IGBT modules in new energy vehicles," *IEEE Trans. Ind. Electron.*, vol. 68, no. 6, pp. 5248-5258, Jun. 2021.

[12] W. Guo, M. Ma, H. Wang, N. Xiang, H. Wang, Z. Chen, and W. Chen, "Real-time average junction temperature estimation for multichip IGBT modules with low computational cost," *IEEE Trans. Ind. Electron.*, vol. 70, no. 4, pp. 4175-4185, Apr. 2023.

[13] Z. Khatir, "Junction temperature investigations based on a general semi-analytical formulation of forward voltage of power diodes," *IEEE Trans. Electron Devices*, vol. 59, no. 6, pp. 1716-1722, Jun. 2012.

[14] A. Arya, A. Chanekar, P. Deshmukh, A. Verma, and S. Anand, "Accurate online junction temperature estimation of IGBT using inflection point based updated I-V characteristics," *IEEE Trans. Power Electron.*, vol. 36, no. 9, pp. 9826-9836, Sep. 2021.

[15] Y. Yang, Q. Zhang, and P. Zhang, "A fast IGBT junction temperature estimation approach based on on-state voltage drop," *IEEE Trans. Ind. Appl.*, vol. 57, no. 1, pp. 685-693, Jan./Feb. 2021.

[16] S. Cheng, Y. Hu, C. Xiang, J. Liu, X. Wu, and J. Yao, "An online condition monitor method for IGBT independent of collector current," *IEEE Trans. Transp. Electrif.*, vol. 8, no. 4, pp. 4607-4621, Dec. 2022.

[17] Z. Xu, F. Xu, and F. Wang, "Junction temperature measurement of IGBTs using short-circuit current as a temperature-sensitive electrical parameter for converter prototype evaluation," *IEEE Trans. Ind. Electron.*, vol. 62, no. 6, pp. 3419-3429, Jun. 2015.

[18] Y. Yang and P. Zhang, "A novel converter-level IGBT junction temperature estimation method based on the bus voltage ringing," *IEEE Trans. Power Electron.*, vol. 37, no. 4, pp. 4553-4563, Apr. 2022.

[19] Y. Peng, Q. Wang, H. Wang, and H. Wang, "An on-line calibration method for TSEP-based junction temperature estimation," *IEEE Trans. Ind. Electron.*, vol. 69, no. 12, pp. 13616-13624, Dec. 2022.

[20] W. Lai, Y. Wei, M. Chen, H. Xia, D. Luo, H. Li, J. Zhang, and H. Li, "In-situ calibration method of online junction temperature estimation in IGBTs for electric vehicle drives," *IEEE Trans. Power Electron.*, vol. 38, no. 1, pp. 1178-1189, Jan. 2023.

[21] Y. Chen, H. Luo, W. Li, X. He, F. Iannuzzo, and F. Blaabjerg, "Analytical and experimental investigation on a dynamic thermo-sensitive electrical parameter with maximum dI_c/dt during turn-off for high power trench gate/field-stop IGBT modules," *IEEE Trans. Power Electron.*, vol. 32, no. 8, pp. 6394-6404, Aug. 2017.

[22] H. Luo, Y. Chen, P. Sun, W. Li, and X. He, "Junction temperature extraction approach with turn-off delay time for high-voltage high-power IGBT modules," *IEEE Trans. Power Electron.*, vol. 31, no. 7, pp. 5122-5132, Jul. 2016.

[23] Q. Zhang and P. Zhang, "An online junction temperature monitoring method for SiC MOSFETs based on a novel gate conduction model," *IEEE Trans. Power Electron.*, vol. 36, no. 10, pp. 11087-11096, Oct. 2021.

[24] X. Jiang, J. Wang, H. Yu, J. Chen, Z. Zeng, X. Yang, and Z. Shen, "Online junction temperature measurement for SiC MOSFET based on dynamic threshold voltage extraction," *IEEE Trans. Power Electron.*, vol. 36, no. 4, pp. 3757-3768, Apr. 2021.

[25] N. Baker and F. Iannuzzo, "The temperature dependence of the flatband voltage in high-power IGBTs," *IEEE Trans. Ind. Electron.*, vol. 66, no. 7, pp. 5581-5584, Jul. 2019.

[26] R. Mandeya, C. Chen, V. Pickert, R. T. Naayagi, and B. Ji, "Gate-emitter pre-threshold voltage as a health-sensitive parameter for IGBT chip failure monitoring in high-voltage multichip IGBT power modules," *IEEE Trans. Power Electron.*, vol. 34, no. 9, pp. 9158-9169, Sep. 2019.

[27] C. H. van der Broeck, A. Gospodinov, and R. W. De Doncker, "IGBT junction temperature estimation via gate voltage plateau sensing," *IEEE Trans. Ind. Appl.*, vol. 54, no. 5, pp. 4752-4763, Sep./Oct. 2018.

[28] Y. Yang and P. Zhang, "In situ insulated gate bipolar transistor junction temperature estimation method via a bond wire degradation independent parameter turn-off V_{ce} overshoot," *IEEE Trans. Ind. Electron.*, vol. 68, no. 10, pp. 10118-10129, Oct. 2021.

[29] L. Shao, G. Xu, L. Zheng, Z. Pan, and C. She, "IGBT junction temperature extraction via voltage integral over voltage rise period," *IEEE J. Emerg. Sel. Top. Power Electron.*, 2022, early access.

[30] Q. Zhang, G. Lu, and P. Zhang, "A high-sensitivity online junction temperature monitoring method for SiC MOSFETs based on the turn-on drain-source current overshoot," *IEEE Trans. Power Electron.*, vol. 37, no. 12, pp. 15505-15516, Dec. 2022.

[31] A. Bryant, S. Yang, P. Mawby, D. Xiang, L. Ran, P. Tavner, and P. R. Palmer, "Investigation into IGBT dV/dt during turn-off and its temperature dependence," *IEEE Trans. Power Electron.*, vol. 26, no. 10, pp. 3019-3031, Oct. 2011.

[32] Y. Zhang, J. Fang, F. Gao, T. Song, S. Gao, and D. J. Rogers, "Second-harmonic ripple voltage suppression of integrated single-phase pulsewidth modulation rectifier charging system for EVs," *IEEE Trans. Power Electron.*, vol. 35, no. 4, pp. 3616-3626, Apr. 2020.

[33] L. Peng, L. Ma, W. Song, and H. Liu, "A simple model predictive instantaneous current control for single-phase PWM converters in stationary reference frame," *IEEE Trans. Power Electron.*, vol. 37, no. 7, pp. 7629-7639, Jul. 2022.

[34] C. Lin, H. Wang, Q. Deng, X. Ge, D. Liu, D. Xie, and Y. Zuo, "Impact analysis of digital delay on power factor and compensation strategy for electric traction PWM rectifier," *IEEE J. Emerg. Sel. Top. Power Electron.*, early access.

[35] X. Peng, F. Yang, G.Wang, Y. Wu, L. Li, Z. Li, A. A. Bhatti, C. Zhou, D. M. Hepburn, A. J. Reid, M. D. Judd, and W. H. Siew, "A convolutional neural network-based deep learning methodology for recognition of partial discharge patterns from high-voltage cables," *IEEE Trans. Power Deliv.*, vol. 34, no. 4, pp. 1460-1469, Aug. 2019.

[36] H. Li, S. R. Lee, M. Luo, C. R. Sullivan, Y. Chen, and M. Chen, "MagNet: A machine learnig framework for magnetic core loss modeling," in *Proc. COMPEL 2020*, 2020, pp. 1-8.